

pubs.acs.org/JACS Article

Programming DNA Self-Assembly by Geometry[†]

Cuizheng Zhang, Mengxi Zheng, Yoel P. Ohayon, Simon Vecchioni, Ruojie Sha, Nadrian C. Seeman, Natasha Jonoska,* and Chengde Mao*



Cite This: J. Am. Chem. Soc. 2022, 144, 8741-8745



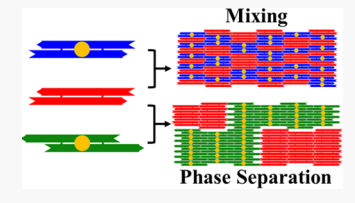
ACCESS

III Metrics & More

Article Recommendations

Supporting Information

ABSTRACT: This manuscript introduces geometry as a means to program the tile-based DNA self-assembly in two and three dimensions. This strategy complements the sequence-focused programmable assembly. DNA crystal assembly critically relies on intermotif, sticky-end cohesion, which requires complementarity not only in sequence but also in geometry. For DNA motifs to assemble into crystals, they must be associated with each other in the proper geometry and orientation to ensure that geometric hindrance does not prevent sticky ends from associating. For DNA motifs with exactly the same pair of sticky-end sequences, by adjusting the length (thus,



helical twisting phase) of the motif branches, it is possible to program the assembly of these distinct motifs to either mix with one another, to self-sort and consequently separate from one another, or to be alternatingly arranged. We demonstrate the ability to program homogeneous crystals, DNA "alloy" crystals, and definable grain boundaries through self-assembly. We believe that the integration of this strategy and conventional sequence-focused assembly strategy could further expand the programming versatility of DNA self-assembly.

INTRODUCTION

The length (and, consequently, the twist) of helical domains represents a primary consideration in designing DNA nanoscale motifs in accordance with the helical nature of the DNA duplex [10.5 base pairs (bp) per turn].^{1,2} For example, in the double-crossover (DX) molecule, the distance between two crossover points needs to be an integer number of half helical turns to ensure that the two-component duplexes are aligned on the same plane.³ When DX molecules self-assemble into two-dimensional (2D) crystals, the same requirement must be met for the separation between the crossover points of any two associated DX molecules.4 This requirement is equally important for the self-assembly of three-dimensional (3D) DNA crystals.⁵ However, to date, this geometry component has not been actively explored as a programming tool for selfassembly; instead, self-assembly via sequence complementarity has been primarily used.⁶⁻⁸ We hypothesize here that geometry could also be employed in addition to or as an alternative driving force to sequence to program DNA selfassembly. Using proper geometric alignment, DNA tiles can fit together to allow all complementary sticky ends in the system to hybridize. In the context of improper geometric compatibility, DNA tiles cannot fully reach each other, thus leaving some sticky ends unpaired, which would generate a high-energy, unstable state. To minimize the free energy, the tiles would avoid the wrong geometry and instead arrange themselves into the correct, designed geometry. Herein, we have demonstrated this concept in tile-based self-assembly of both 2D and 3D DNA crystals.

RESULTS AND DISCUSSION

We first tested geometry-based programing in the assembly of 2D DX crystals (Figure 1). Three DAE-O tiles containing a 2fold rotational symmetry were designed as follows: P (plain), M (mixing), and S (separation). DAE-O stands for antiparallel double-crossover molecules with an even number of half-turns (4 half-turns, 21 bp) between the two crossover points within each tile. When individual tiles assemble into homogeneous 2D arrays, the distance between two crossover points from two adjacent tiles is an odd number of half-turns (27 bp, corresponding to 5 half-turns).3 With such tiles, the tiles along any continuous DNA helix will alternatingly face up and down, thus canceling any potential curvature along the long axis of the tiles and driving the tiles to assemble into extended crystals. Different from tile P, tiles M and S both have a pair of hairpins extruding from the tile planes. Those hairpins serve as tomographic markers in atomic force microscopy (AFM) images to distinguish tiles M and S from tiles P. All three tiles have the same pair of 5 nt long sticky ends represented as either geometry-matched arrowheads or arrow tails. Two like tiles associate with each other via sticky-end cohesion, and the distance between two adjacent crossover points will be 27 bp, near 2.5 turns (26.3 bp), corresponding to ~180° rotation around the DNA helix. This leads to the two tiles being on the

Received: March 4, 2022 Published: May 4, 2022





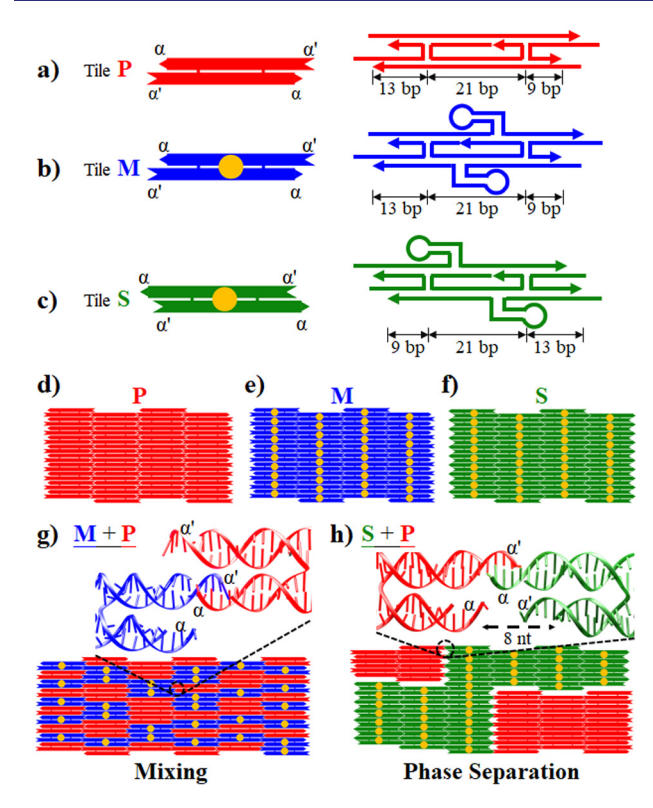


Figure 1. Geometry-controlled self-assembly of 2D DNA crystals using DX molecules. (a–c) Designs of three symmetric DX tiles **P**, **M**, and **S**, standing for plain, mixing, and separation, respectively. They have the same pair of 5 nt long sticky ends (α and α'). Left are simple schemes. The solid rods and circles represent DNA duplexes and hairpins, respectively; the geometric complementarity of the rod ends represents the sequence complementarity of sticky ends. (d–f) Homogeneous 2D DX crystals from individual tiles. (g) Alloy 2D crystals expected from the mixture of tiles **M** and **P**. (h) Phase separation expected from the mixture of tiles **S** and **P**.

same plane but facing opposite directions. Thus, separately, each type of DX tile can self-assemble into homogeneous 2D crystals (Figure 1d-f).

Tiles P and M have the same structure, except for the presence of hairpins in tile M. Thus, it is expected that these two types of tiles can coassemble into 2D crystals, in which they are randomly mixed like in alloys (Figure 1g). Their distribution can be readily examined due to the extra hairpins (appearing tall spots in AFM images) of tile M. By contrast, tile S is geometrically different from tiles P and M: the lengths of the four helical domains outside of the crossover points in tile S are different from those in tiles P and M. When an S tile and a P tile associate via sticky-end cohesion, the distance between two adjacent crossover points from the two tiles will be either 23 or 31 bp, quite far from 2.5 turns (26.3 bp), resulting in a state where the two tiles are not in the same plane. Such nonplanar association prevents the assembly of tiles P and S into continuous, heterogeneous 2D crystals. Instead, the two types of tiles will self-assemble into separate domains with each domain containing only one type of tile (Figure 1h). Such a phase separation phenomenon would easily be observable in AFM images, as the domains of tile P are plain, and the domains of tile S have hairpins.

An experimental study has confirmed that we can control the assembly of DNA tiles based on their geometry, even though the tiles have the same sticky ends (Figure 2). Each individual

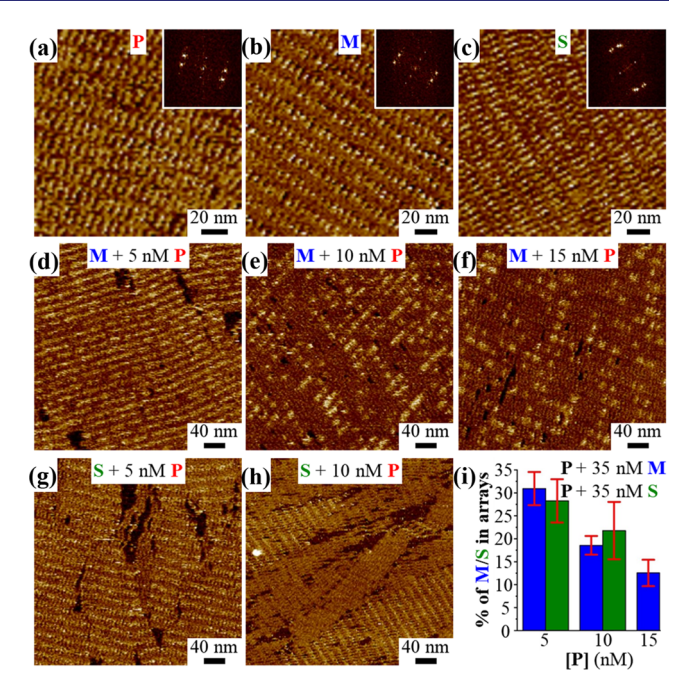


Figure 2. AFM images of 2D DNA arrays assembled on mica surfaces: (a) from tile P(25 nM); (b) from tile M(35 nM); and (c) from tile S(35 nM). Insets show corresponding FFT patterns. From the mixture of tile M(35 nM) with tile P at (d) S nM, (e) S nM, and (f) S nM. From the mixture of tile S(35 nM) with tile S nM with tile S nM and (h) S nM (i) Occupancy of hairpin tiles (M or S) in the 2D arrays observed in AFM images. Red lines represent the standard deviations (S nM nM).

tile could readily form (Figures S1–S3) and self-assemble into homogeneous, periodic 2D arrays (Figures 2a–c and S4). The brighter regions in the AFM images in Figure 2b,c show the hairpins of tiles **M** and **S** extruding from the planes. The regularity of the arrays was evidenced by the ensuing fast Fourier transform (FFT) patterns. The repeating, interhairpin distances were consistent between the measured values (14.9 nm in Figure 2a for tile **P** array, 16.1 nm in Figure 2b for tile **M** array, and 16.7 nm in Figure 2c for tile **S** array) and the calculated value (15.5 nm) from the design, assuming 0.34 nm/bp.

Either tile mixing or tile separation was observed when two different tiles were mixed in a single pot as discussed above. (i) When tiles M and P were mixed (Figures 2d-f and S5), 2D DNA arrays readily formed. In the arrays, brighter spots (corresponding hairpins of tile M) were randomly distributed, indicating that the two tiles were randomly mixed and the 2D arrays were DNA alloys. The hairpin density decreased as the relative fraction of the hairpin-containing tile M in the assembly solution decreased. (ii) When tiles S and P were mixed (Figures 2g,h and S6), 2D DNA arrays readily formed as well. However, the brighter spots (hairpins, corresponding to tile S) were no longer randomly distributed; instead, the brighter spots were aggregated. In the arrays, some domains were hairpin-rich, while other domains were hairpin-deficient. This observation indicated the phenomenon of self-sorting: like tiles tended to associate and unlike tiles did not; thus, phase separation was achieved. The ratio between the two types of domains depended on the relative concentrations of the tiles in the initial assembly solution. The separations containing larger regions of self-sorted assemblies with tiles P

(nonhairpin labeled) were observed in Figure 2h, where an increased concentration of these tiles was present.

To quantitatively distinguish between tile mixing and separation, we compared the variation in hairpin content across different regions of the AFM images. For the DNA alloys (in the case of tile mixing), hairpins were uniformly and randomly distributed, and their content had little variation over different areas of the arrays. In contrast, for phase separation, the hairpin content fluctuated greatly. The local distribution was nearly 0 and 100% in the domains of tiles P and S, respectively. Large-area AFM images of the 2D DNA arrays coassembled from tiles M and P (Figure S7) and tiles S and P (Figure S8) were divided into nine sections of equal size. The hairpin content in each section was measured. For the nine sections of each large AFM image, we then calculated the average hairpin content and its standard deviation (which indicated the content variation). As summarized in Figure 2i, arrays from tiles S and P always had a much higher standard deviation of hairpin content than arrays from tiles M and P. When the concentration of tile P was too low (5 nM), after mixing with either tile M or S, almost the entire area contained hairpins. In these arrays, it was difficult to employ this statistical method to determine the difference between uniformly distributed structures and self-sorting structures, although these structures could also be observed in some small areas (Figure 2d,g). When the concentration of the P tile was increased to 10 nM, the results showed a significant statistical difference. For the mixture of tiles M and P, the hairpin distribution was uniform, and the hairpin content had a standard deviation of 2.0% (Figures 2e and S7). In contrast, for the mixture of tiles S and P, the standard deviation of the hairpin content increased dramatically to 6.2% (Figures 2h and S8). When the concentration of tile P was further increased to 15 nM, the statistical difference became more obvious. For the mixture of tiles M and P, the average coverage of hairpins in nine sections was 12.6% and the distribution remained uniform (Figure 2f). By contrast, when the mixture of tiles S and P was completely separated into phases, only tile P could be observed at this ratio (Figure S6c).

Programming of DNA assembly by geometry is generally applicable. To demonstrate the generalizability of this technique, we tested it on two other systems. The first system is a coassembly of two symmetric DAE tiles (LB and LH) into 2D arrays, wherein each tile will assemble into one-dimensional (1D) fibers on its own (Figure 3). They share the same pair of complementary sticky ends. Tile LB is plain, but tile LH contains hairpins (which serve as the tomographic markers to distinguish these two different tiles in AFM images). When two tiles of the same type associate, their center-to-center distance will, respectively, be 21 + 9 + 5 + 9 = 44 bp for tile LB and 21 + 12 + 5 + 12 = 50 bp for tile LH. The corresponding rotational angles along DNA duplexes are, respectively, 69° for tile LB and 86° for tile LH when assuming 360°/10.5 bp. Such angles place the associated tiles on different planes; thus, none of the tiles in isolation can self-assemble into continuous 2D arrays. Instead, each tile alone will associate with 1D fibers. In the fibers, tiles pair with neighboring tiles by twisting 69 and 86° compared with the B-type DNA (indicating a high-energy, or only metastable, state). By contrast, if tiles LB and LH assemble alternatingly, the center-to-center distance between tiles will be 21 + 12 + 5 + 9 = 47 bp, corresponding to a rotational angle of 171° (~180°). Thus, the tiles will be roughly on the same plane, thereby generating continuous 2D

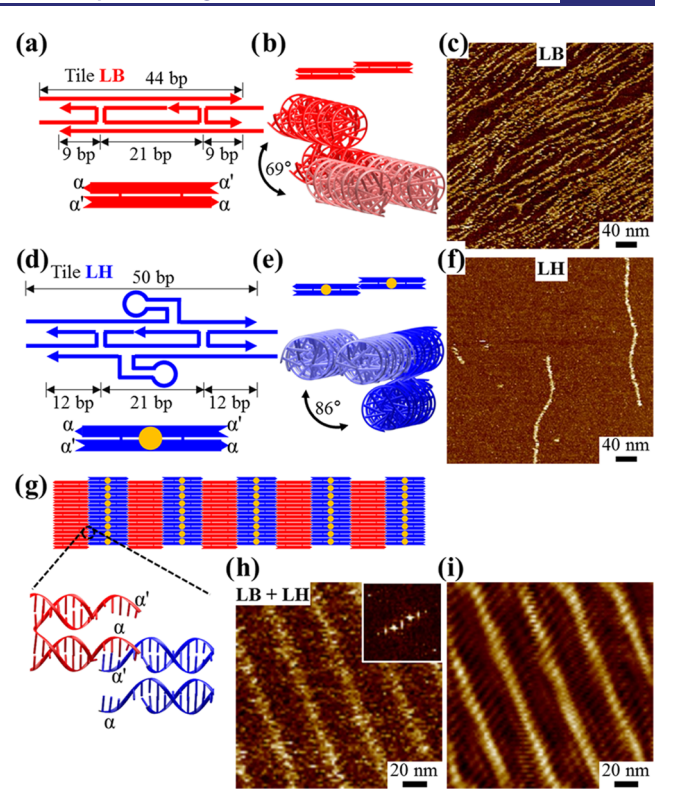


Figure 3. Self-assembly of 2D DNA arrays with an alternating tile arrangement. Tiles (a–c) LB and (d–f) LH separately assembled into 1D fibers but (g–i) together coassembled into alternating 2D arrays. (a, d) Designs of the individual tiles. (b, e) Association of the two like tiles leads to nonplanar complexes. (g) Alternating arrangement of tiles LB and LH into 2D arrays. The AFM images of the assembly of tiles (c) LB (25 nM) and (f) LH (65 nM) separately. (h) AFM image and (i) its FFT reconstructed image of the 2D arrays coassembled from tiles LB (25 nM) and LH (65 nM) together. The inset in (h) is the corresponding FFT pattern.

crystals. As all sticky ends are base paired, the resulting 2D crystals become more stable due to a lower energy state. This reasoning was verified experimentally (Figures 3 and S9–S11). In the AFM images, only 1D fibers were observed from either tile alone (Figures 3c and S11a for tile LB; Figures 3f and S11b for tile LH), and well-ordered, continuous 2D arrays were assembled from the mixture of tiles LB and LH (Figures 3h,i and S11c). The measured distance (33.6 nm) between the hairpin strips in the 2D arrays was in agreement with the calculated distance (32.0 nm) between the hairpins from the adjacent tiles along connecting DNA duplexes in the 2D arrays, where tiles LB and LH were arranged alternatingly.

The third system that examined employing geometric strategy in 3D self-assembly (Figure 4) used three different, four-turn, symmetric, triangle motifs (T) (Figures S12–S16).⁵ Each triangle consists of seven strands: one central black strand, three copies of identical cyan strands, and three copies of identical red strands. All three motifs share the same pair of 2 nt sticky ends. However, the lengths of the attachment arms (beyond the junction points) of the triangles are different though the length of each side duplex remains the same (42 bp). Each individual motif alone could readily assemble into 3D crystals because the repeating distance along any DNA duplex is an integer number of helical turns, 4 in our case (Figures 4a, S15, and S16). When mixed together, the motifs exhibited clear self-sorting behavior in assembly, even though

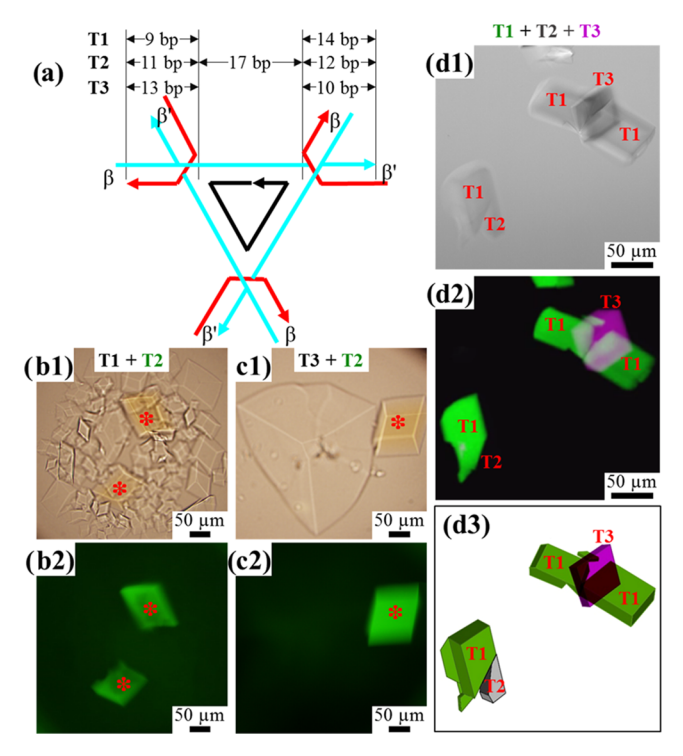


Figure 4. Geometry-controlled self-sorting in 3D crystallization of symmetric triangle motifs (T). (a) Structure scheme of three motifs (T1, T2, and T3). All motifs contain the same pair of 2 nt sticky ends (β and β). The crystal drops of the mixtures of (b) 1.2 μ M T1 + 0.3 μ M T2 and (c) 1.2 μ M T3 + 0.3 μ M T2. The central black strand of T2 is modified with 6-FAM. Panels (b1) and (c1) optical images; (b2) and (c2) corresponding fluorescence images. Red asterisks indicate fluorescence-labeled crystals. (d1) Transmitted light image, (d2) a reconstructed confocal microscopy image, and (d3) a schematic showing of a crystal drop of the mixture of 0.5 μ M T1 + 0.5 μ M T2 + 0.5 μ M T3. The central strands of T1 and T3 are modified with 6-FAM and Cy5, respectively.

they had the same sticky ends (Figures 4b-d, S17, and S18). Association between any two unlike motifs will result in a wrong geometry: the two motifs have a relative rotation around the connecting duplex in addition to translation; in this way, they cannot further assemble into periodic 3D crystals. When unlabeled motif T1 (1.2 μ M) and green fluorescence (6-FAM)-labeled motif T2 (0.3 μ M) were mixed, crystals appeared (Figure 4b) having either a strong green fluorescence or a complete lack thereof. No mixture of fluorescent and nonfluorescent parts in the same crystal was observed. The identical phenomenon occurred when unlabeled motif T3 (1.2 μ M) and 6-FAM-labeled motif T2 (0.3 μ M) were mixed (Figure 4c). In some cases, multiple crystals adhered together at the surface (3D grain boundary). After enzymatically ligating the crystals⁹ and subsequently crushing the crystal agglomerates, each individual crystal piece showed homogeneity in having either fluorescence or complete lack thereof (Figure S18). Furthermore, triple-phase separation occurred when assembling crystals from the mixture of all three motifs [unlabeled T2, 6-FAM-labeled T1, and purple fluorescence (Cy5)-labeled T3] at an equal concentration (0.5 μ M). This multiphase separation was easily visualized by confocal microscopy (Figure 4d). It was clear that the three motifs did not mix with each other into alloy crystals despite the fact that they shared common sticky ends. Instead, they self-sorted

to assemble into homogeneous single-motif crystals as a result of geometric driving forces.

CONCLUSIONS

In summary, we have developed a strategy to program DNA self-assembly based on tile geometry in addition to the commonly used, sticky-end approach. The geometry provides an orthogonal tool for the programmability of DNA self-assembly using diverse, tile-based components. It is reasonable to envision that a simultaneous control of both tile geometry and sticky-end sequence would expand our programming capabilities and increase the assembly fidelity, both of which are critically important for robust DNA nanoconstruction, ^{10–13} algorithmic DNA assembly, ^{6,8,14,15} and DNA-based information processing and storage. ^{16–19} This strategy will also contribute to the construction of DNA-based sensors ^{20–24} with high sensitivity and accuracy.

ASSOCIATED CONTENT

Supporting Information

The Supporting Information is available free of charge at https://pubs.acs.org/doi/10.1021/jacs.2c02456.

Detailed experimental methods and additional experimental data (PDF)

AUTHOR INFORMATION

Corresponding Authors

Ruojie Sha — Department of Chemistry, New York University, New York, New York 10003, United States; ocid.org/ 0000-0002-0807-734X; Email: rs17@nyu.edu

Natasha Jonoska — Department of Mathematics and Statistics, University of South Florida, Tampa, Florida 33620, United States; Email: jonoska@mail.usf.edu

Chengde Mao – Department of Chemistry, Purdue University, West Lafayette, Indiana 47907, United States; oorcid.org/0000-0001-7516-8666; Email: mao@purdue.edu

Authors

Cuizheng Zhang — Department of Chemistry, Purdue University, West Lafayette, Indiana 47907, United States Mengxi Zheng — Department of Chemistry, Purdue University, West Lafayette, Indiana 47907, United States; orcid.org/ 0000-0002-1625-6663

Yoel P. Ohayon — Department of Chemistry, New York University, New York, New York 10003, United States
Simon Vecchioni — Department of Chemistry, New York
University, New York, New York 10003, United States
Nadrian C. Seeman — Department of Chemistry, New York
University, New York, New York 10003, United States;
orcid.org/0000-0002-9680-4649

Complete contact information is available at: https://pubs.acs.org/10.1021/jacs.2c02456

Author Contributions

¹C.Z. and M.Z. contributed equally to this work.

Notes

The authors declare no competing financial interest.

ACKNOWLEDGMENTS

This work was financially supported by NSF (CCF-2107393 to C.M.; 2106790 to Y.P.O., N.C.S., and R.S.; 2107267 to N.J.; and CCMI- 2025187 to C.M.).

DEDICATION

[†]In memory of Prof. Nadrian C. Seeman who passed away during the preparation of this manuscript on November 16, 2021.

REFERENCES

- (1) Watson, J. D.; Crick, F. C. H. Crick. Molecular structure of nucleic acids: a structure for deoxyribose nucleic acid. *Nature* **1953**, 171, 737–738.
- (2) Wang, J. C. Helical repeat of DNA in solution. *Proc. Natl. Acad. Sci. U.S.A.* **1979**, *76*, 200–203.
- (3) Fu, T. J.; Seeman, N. C. DNA double-crossover molecules. *Biochemistry* **1993**, 32, 3211–3220.
- (4) Winfree, E.; Liu, F.; Wenzler, L. A.; Seeman, N. C. Design and self-assembly of two-dimensional DNA crystals. *Nature* **1998**, 394, 539–544
- (5) Zheng, J.; Birktoft, J. J.; Chen, Y.; Wang, T.; Sha, R.; Constantinou, P. E.; Ginell, S. L.; Mao, C.; Seeman, N. C. From molecular to macroscopic via the rational design of a self-assembled 3D DNA crystal. *Nature* **2009**, *461*, 74–77.
- (6) Rothemund, P. W. K.; Papadakis, N.; Winfree, E. Algorithmic self-assembly of DNA Sierpinski triangles. *PLoS Biol.* **2004**, *2*, No. e424.
- (7) Evans, C. G.; Winfree, E. Physical principles for DNA tile self-assembly. *Chem. Soc. Rev.* **2017**, *46*, 3808–3829.
- (8) Woods, D.; Doty, D.; Myhrvold, C.; Hui, J.; Zhou, F.; Yin, P.; Winfree, E. Diverse and robust molecular algorithms using reprogrammable DNA self-assembly. *Nature* **2019**, 567, 366–372.
- (9) Li, Z.; Liu, L.; Zheng, M.; Zhao, J.; Seeman, N. C.; Mao, C. Making engineered 3D DNA crystals robust. *J. Am. Chem. Soc.* **2019**, 141, 15850–15855.
- (10) Pinheiro, A. V.; Han, D.; Shih, W. M.; Yan, H. Challenges and opportunities for structural DNA nanotechnology. *Nat. Nanotechnol.* **2011**, *6*, 763–772.
- (11) Wang, P.; Meyer, T. A.; Pan, V.; Dutta, P. K.; Ke, Y. The beauty and utility of DNA origami. *Chem* 2017, 2, 359–382.
- (12) Seeman, N. C.; Sleiman, H. F. DNA nanotechnology. *Nat. Rev. Mater.* **2018**, *3*, No. 17068.
- (13) Hu, Q.; Li, H.; Wang, L.; Gu, H.; Fan, C. DNA nanotechnology-enabled drug delivery systems. *Chem. Rev.* **2019**, 119, 6459–6506.
- (14) Cho, H.; Mitta, S. B.; Song, Y.; Son, J.; Park, S.; Ha, T. H.; Park, S. H. 3-Input/1-output logic implementation demonstrated by DNA algorithmic self-assembly. *ACS Nano* **2018**, *12*, 4369–4377.
- (15) Tandon, A.; Song, Y.; Mitta, S. B.; Yoo, S.; Park, S.; Lee, S.; Raza, M. T.; Ha, T. H.; Park, S. H. Demonstration of arithmetic calculations by DNA tile-based algorithmic self-assembly. *ACS Nano* **2020**, *14*, 5260–5267.
- (16) Qian, L.; Winfree, E. Scaling up digital circuit computation with DNA strand displacement cascades. *Science* **2011**, 332, 1196–1201
- (17) Qian, L.; Winfree, E.; Bruck, J. Neural network computation with DNA strand displacement cascades. *Nature* **2011**, *475*, 368–372.
- (18) Zhang, D. Y.; Seelig, G. Dynamic DNA nanotechnology using strand-displacement reactions. *Nat. Chem.* **2011**, *3*, 103–113.
- (19) Ceze, L.; Nivala, J.; Strauss, K. Molecular digital data storage using DNA. *Nat. Rev. Genet.* **2019**, *20*, 456–466.
- (20) Krishnan, Y.; Simmel, F. C. Nucleic acid based molecular devices. *Angew. Chem., Int. Ed.* **2011**, *50*, 3124–3156.
- (21) Li, J.; Mo, L.; Lu, C.-H.; Fu, T.; Yang, H.-H.; Tan, W. Functional nucleic acid-based hydrogels for bioanalytical and biomedical applications. *Chem. Soc. Rev.* **2016**, *45*, 1410–1431.
- (22) Zhou, W.; Saran, R.; Liu, J. Metal sensing by DNA. Chem. Rev. 2017, 117, 8272-8325.
- (23) Schneider, A.-K.; Niemeyer, C. M. DNA surface technology: from gene sensors to integrated systems for life and materials sciences. *Angew. Chem., Int. Ed.* **2018**, *57*, 16959–16967.

(24) Nicolson, F.; Ali, A.; Kircher, M. F.; Pal, S. DNA nanostructures and DNA-functionalized nanoparticles for cancer theranostics. *Adv. Sci.* **2020**, *7*, No. 2001669.

□ Recommended by ACS

Programming 2D Supramolecular Assemblies with Wireframe DNA Origami

Xiao Wang, Mark Bathe, et al.

MARCH 01, 2022

JOURNAL OF THE AMERICAN CHEMICAL SOCIETY

READ 🗹

Developmental Self-Assembly of a DNA Ring with Stimulus-Responsive Size and Growth Direction

Allison T. Glynn, Lulu Qian, et al.

MAY 26, 2022

JOURNAL OF THE AMERICAN CHEMICAL SOCIETY

READ 🗹

Making Engineered 3D DNA Crystals Robust

Zhe Li, Chengde Mao, et al.

SEPTEMBER 25, 2019

JOURNAL OF THE AMERICAN CHEMICAL SOCIETY

READ 🗹

Hierarchical Assembly of Super-DNA Origami Based on a Flexible and Covalent-Bound Branched DNA Structure

Yan Li, Baoquan Ding, et al.

NOVEMBER 16, 2021

JOURNAL OF THE AMERICAN CHEMICAL SOCIETY

READ **C**

Get More Suggestions >